Transverse modes and beam spatial quality in microchip lasers

Matas Plukys ,[1,*] Eugenijus Gaizauskas ,[1] Darius Gailevicius,[1] and Kestutis Staliunas[1,2,3]

[1]*Laser Research Center, Faculty of Physics, Vilnius University, Sauletekio Avenue 10, Vilnius LT-10223, Lithuania*

[2]*ICREA, Passeig Lluís Companys 23, 08010 Barcelona, Spain*

[3]*Departament de Fisica, Universitat Politècnica de Catalunya, Rambla Sant Nebridi 22, 08222 Terrassa (Barcelona), Spain*

(Received 29 August 2022; accepted 27 March 2023; published 20 April 2023)

We analyze the transverse modes in flat-flat mirror microchip-laser resonators, which occur due to the gain guiding and the thermal lensing. We rigorously calculate the transverse-mode functions, their eigenfrequencies, and their generation-threshold conditions. We apply a plausible assumption that the mode amplitudes in multi-transverse-mode emission are proportional to the individual gain factors of each mode, and we estimate the beam quality factor for the multi-transverse-mode emission. This simple and intuitive approach leads to the beam quality estimations corresponding well to the experimental measurements performed here.

DOI: 10.1103/PhysRevA.107.043505

I. INTRODUCTION

The well-established classical optical resonator theory explicitly defines the transverse modes arising in resonators built from curved mirrors. In that case, the solutions satisfy the paraxial approximation of the scalar wave equation and take the shape of the Gauss-Hermite or Gauss-Laguerre function. These mode solutions, mathematically speaking, are the eigenfunctions of the resonator wave equations and, physically speaking, reproduce themselves after each round trip in a resonator (see, e.g., [1,2] for a review). The classical theory considers an idealized resonator operating close to the generation threshold without gain-saturation and gain-guiding effects. The transverse light dynamics in such resonators is analogous to the dynamics of a wave function in a parabolic potential well (the solution of the Schrödinger equation for a quantum harmonic oscillator) as described in textbooks of quantum mechanics.

In many relevant cases, particularly for large pump powers, i.e., highly nonlinear regimes, the transverse-mode description becomes very approximate or even ceases to work [3–5]. The investigation of transverse modes in the nonlinear regime is still the subject of current research [6,7]. For some special lasers, like microchip lasers, the classical mode theory is barely applicable from the very beginning because their resonators consist of plano mirrors (see Fig. 1). The parabolic trapping potential is then absent, and the electromagnetic radiation is confined in the transverse space of the resonator by other mechanisms, predominantly by the gain guiding. Thermal lensing also appears to play an important role in confining the radiation in a microchip laser under strong pump power.

The wave-equation solutions for nonspherical mirror resonators were introduced by Siegman [8] even before the concept of a microchip laser was established. After the experimental demonstration of the effectiveness of microchip lasers [9], a dedicated theoretical investigation of end-pumped solid-state microchip lasers began [10]. In order to reduce the problem complexity, the transverse pumping profile was approximated as an infinite parabola, which authors himself described as unphysical. Further investigations [11–14] considered transverse-mode behavior with localized gain profiles and treated the problem only in one dimension. The significant works in [15,16] combined the theoretical investigation with experiment, in which the gain and index profiles were approximated as Gaussian and parabolic, respectively. The latter approach does not help to find the solutions analytically; eigenstates have to be calculated purely numerically. Also, the thermally induced lens modulates the phase logarithmically outside the pumping region [17], and the parabolical approximation is rather ideally suited for a resonator with curved output couplers. It is worth mentioning that in addition to the solid-state microchip, vertical-cavity surface-emitting lasers can have a plano-plano mirror configuration. The theoretical investigation of such lasers [18–20] calculated the gain profile numerically from the carrier-diffusion equation. Then the transversal modes were calculated numerically as in

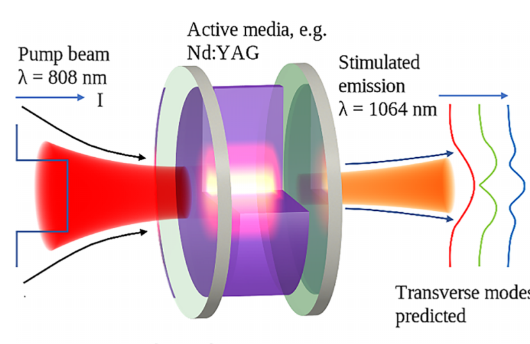

FIG. 1. Schematic drawing of an end-pumped microchip laser with the guiding section induced by the pump beam.

*matas.plukys@ff.vu.lt

 ©2023 American Physical Society

a solid-state microchip [15]. However, the severest drawback of the mentioned investigations [10–16,18–20] is the failure to provide a plausible picture of the multimode emission of such a laser. Rigorous nonlinear calculations are very complicated even in the single-longitudinal-mode case (so-called mean-field approximation; see, for instance, [4]) and are hardly possible in full multi-transverse-, multi-longitudinal-mode description. Therefore, the absence of a simple method to calculate the beam-radiation profiles forces laser engineers to use some intuitive assumptions about the number of modes supported by the resonator, relating it to the Fresnel number.

This paper aims to fill the gap by providing an analytical and numerical treatment of transverse modes in microchip lasers in two dimensions. Using the cylindrical (flat-top) pumping-profile approach, we provide a simple theory of the gain-guided and thermal-lens-supported modes in such plano-plano mirror resonators. We rigorously calculate the transverse-mode functions, their eigenfrequencies and generation-threshold conditions, and the beam quality factor M^2. All this allows us to estimate the multimode beam (composite) M^2 dependence on pumping strength. Importantly, we apply the assumption of the multi-transverse-mode case considering that the mode amplitudes in multi-transverse-mode emission are proportional to the individual gain of each mode. In this way, we estimate the beam quality factors in the multi-transverse-mode emission depending on the pumping strength. This simple and intuitive approach leads to the beam quality estimations corresponding well to the experimental measurements performed and reported here.

Finally, we note that, usually, reported microchip lasers are made of short resonators with plano-plano mirrors [9–12,21]. However, several reports refer to microchip lasers with short crystals placed in cavities with curved output couplers [15,16,22], with side pumping and moderate cavity length [23]. Such resonators can be dominated by classical phase modulation, where the pumping profile overlaps the classical Gauss-Laguerre modes. For such cases, the gain guiding and thermal lens are only perturbations of classical theories [1,2], and our treatment provided here is not very useful.

II. LINEAR FIELD EQUATION IN TWO DIMENSIONS

We consider a simplified model for the laser resonator, where the gain-guiding and thermal-lensing effects are uniformly distributed over the whole crystal length. In this case, the linear evolution equation for the slowly varying electric-field envelope $A(r, \phi, t)$ in two transversal dimensions reads

$$\frac{\partial A}{\partial t} = -\rho A + id\nabla A + i\sigma(r)A + \gamma(r)A. \tag{1}$$

Here time t is normalized to the cavity round-trip time. The coefficient ρ signifies the total losses per one resonator round trip, with diffraction coefficient $d = L/k$, where L and k are the resonator length and wave number, respectively. Further, we consider the axisymmetrical case, where the thermal $\sigma(r)$ and gain $\gamma(r)$ functions depend only on the radius r.

Equation (1) contains no gain-saturation term, which would allow evaluating the nonlinear dynamics of laser radiation adequately [4]. With this term included, the problem is not universally solvable even in the simplest single-longitudinal-mode approximation. We consider the linear, simplified, nonsaturated laser light dynamics (1), which allows us to calculate exponentially growing and decaying eigensolutions, the transverse modes of the resonator. The calculated eigenvalues allow us to define the threshold and beam quality M^2 of the multimode beam, which consists of individual transverse modes with unequal weights, depending on their growth rates.

We solve Eq. (1) in the polar coordinate system using the usual separation of radial and angular variables in the following form:

$$A(r, \phi) = A_l e^{\lambda t} v(r) e^{i\phi l}, \tag{2}$$

where l stands for the orbital number $l = 0, \pm 1, \pm 2, \dots$ and λ is the separation constant. Substituting (2) into (1), we get

$$r^2 \frac{\partial^2 v}{\partial r^2} + r\frac{\partial v}{\partial r} + r^2 v\left(\frac{i\sigma(r) + \gamma(r) - \lambda - \rho}{id}\right) - l^2 v = 0. \tag{3}$$

The solution $v(r)$ depends on thermal lens and gain functions $\sigma(r)$ and $\gamma(r)$. In order to get the analytical form of $v(r)$ we approximate $\sigma(r)$ and $\gamma(r)$ by adequate functions. Specifically, for the end-pumped microchip laser, due to strong localization and the multimode character of the laser diode pump, the gain profile is approximate to a flat top. The index profile is a solution of the heat equation and depends on the pumping profile. In our case, the index profile is parabolic inside the pumped region and logarithmic outside of it [17]. In order to facilitate the semianalytical treatment, we go with the assumption that the index and gain profiles are flat-top functions:

$$\sigma(r) = \begin{cases} \rho_0 & \text{if } r < R, \\ 0 & \text{if } r > R, \end{cases} \quad \gamma(r) = \begin{cases} G_0 & \text{if } r < R, \\ 0 & \text{if } r > R. \end{cases} \tag{4}$$

The step-index profile may seem counterintuitive because the ideal lens contains parabolic phase modulation. Indeed, the parabolic approximation is ideal for the internal pumping region but undergoes rising deviations moving away from it. The step-index approximation should be a reasonable compromise inside and outside the pumping region. The calculated modes and modal eigenvalues are similar to the ones with the parabolic approximation. However, due to the infinite endings, the parabolic approximation predicts too many modes.

One should note that after introducing the thermal lens and gain cylindrical functions (4) into the linear field equation (3), it becomes analogical to the Schrödinger wave equation with a finite and complex-valued potential well. The separation constant λ also becomes a complex number, and the sign of its real part $\mathrm{Re}(\lambda)$ defines whether the appropriate solution of (2) will grow or decrease. The laser modes are above generation threshold if $\mathrm{Re}(\lambda) > 0$.

Normalizing the radial coordinate r to the radius of the gain profile as $\xi = r/R$, from (4) and (3) we get the two Bessel differential equations of the form

$$\xi^2 \frac{\partial^2 v}{\partial \xi^2} + \xi \frac{\partial v}{\partial \xi} + \xi^2 v \alpha^2 - l^2 v = 0 \quad \text{if } \xi < 1,$$
$$\xi^2 \frac{\partial^2 v}{\partial \xi^2} + \xi \frac{\partial v}{\partial \xi} - \xi^2 v \beta^2 - l^2 v = 0 \quad \text{if } \xi > 1, \tag{5}$$

where complex coefficients α and β are given by

$$\alpha^2 = R^2 \frac{i\rho_0 + G_0 - \lambda - \rho}{id}, \quad \beta^2 = R^2 \frac{\lambda + \rho}{id}. \tag{6}$$

An additional complex-valued coefficient ζ characterizes the complex potential-well depth:

$$\zeta^2 = R^2 \frac{i\rho_0 + G_0}{id}. \tag{7}$$

The three coefficients are interrelated by the equality

$$\zeta^2 = \alpha^2 + \beta^2. \tag{8}$$

The solution of (5) should be finite inside the cylinder ($\xi < 1$) and tend to zero if $\xi \to \infty$ outside the cylinder ($\xi > 1$). The proper solutions are the Bessel function of the first kind $J_l(\alpha\xi)$ and the modified Bessel function of the second kind $K_l(\beta\xi)$, respectively. Both Bessel functions should be equal at $\xi = 1$:

$$v(\xi) = J_l(\alpha\xi) \quad \text{if } \xi < 1,$$
$$v(\xi) = \frac{J_l(\alpha)}{K_l(\beta)} K_l(\beta\xi) \quad \text{if } \xi > 1. \tag{9}$$

The derivatives of $v(\xi)$ at $\xi = 1$ should be equal as well. We can use the recurrence relation [24] to calculate the derivatives:

$$J_l'(\alpha\xi) = \alpha J_{l-1}(\alpha\xi) - \frac{l}{\xi} J_l(\alpha\xi) \quad \text{if } \xi < 1,$$
$$K_l'(\beta\xi) = -\beta K_{l-1}(\beta\xi) - \frac{l}{\xi} K_l(\beta\xi) \quad \text{if } \xi > 1. \tag{10}$$

Combining (9) and (10), we obtain the transcendental equation relating the α and β eigenvalues:

$$\frac{\alpha J_{l-1}(\alpha)}{J_l(\alpha)} = -\frac{\beta K_{l-1}(\beta)}{K_l(\beta)}. \tag{11}$$

Eigenvalues α and β in (11) are complex valued, and they can be found numerically.

III. EIGENVALUES, MODE SHAPES, AND BEAM QUALITY FACTORS M^2

We calculate the complex eigenvalue pairs (ζ, β) numerically from (11), the transcendental equation, expressing α through β and ζ in (8). Due to the orbital number l in (11), one eigenvalue of ζ can correspond to several eigenvalues of β. Furthermore, due to the Bessel oscillatory behavior, each ζ can correspond to several β with the same l. Thus, each eigenvalue β is characterized by two mode numbers (l, m). The physical meaning of the potential depth $|\zeta|$ is related to pumping power. β has no clear physical meaning, while $\mathrm{Re}(i\beta^2)$ is proportional to the growth factor of each single mode $\lambda_{re} + \rho$. On the other hand, $\mathrm{Im}(i\beta^2)$ is proportional to the frequency of each single mode λ_{im}.

We neglect eigenvalues with no physical meaning. The modified Bessel function of the second kind $K_l(\xi\beta)$ tends to zero as $\xi \to \infty$ only if $|\arg(\beta)| < \frac{\pi}{2}$ [24]. On the other hand, $\beta = R\sqrt{\frac{\lambda+\rho}{id}}$, where R, ρ, and d are real and positive. The laser generates only if $\mathrm{Re}(\lambda) > 0$; therefore, the β argument is restricted to $-\frac{\pi}{2} < \arg(\beta) < 0$ and $\frac{\pi}{2} < \arg(\beta) < \pi$. Combining these results with the previous restriction, we can finally state that β is valid only if $-\frac{\pi}{2} < \arg(\beta) < 0$.

The potential-well depth $\zeta = R\sqrt{\frac{\rho_0}{d} - i\frac{G_0}{d}}$ depends on the real-valued positive G_0 and the real-valued (but not necessarily positive) ρ_0. Therefore, the phase of ζ is restricted to areas of $-\frac{\pi}{2} < \arg(\zeta) < 0$ and $\frac{\pi}{2} < \arg(\zeta) < \pi$. However, only the area of $-\frac{\pi}{2} < \arg(\zeta) < 0$ is relevant because the two areas overlap using the square of ζ in Eq. (8). One can distinguish several important cases determined by the phase of the potential depth ζ:

(i) If $\rho_0 = 0$, then $\arg(\zeta) = -\frac{\pi}{4}$ is a pure-gain-guiding case, where no phase modulation (lens) is present.

(ii) If $\rho_0 > 0$, then $-\frac{\pi}{4} < \arg(\zeta) < 0$. This case is a mix of gain guiding and focusing lens (approximated as a cylinder). The focusing lens starts to dominate as the phase approaches zero.

(iii) If $\rho_0 < 0$, then $-\frac{\pi}{2} < \arg(\zeta) < -\frac{\pi}{4}$. This case corresponds to a mix of a defocusing lens with gain guiding. The defocusing-lens effect gets stronger as the phase approaches $-\frac{\pi}{2}$.

In order to grasp the dynamics, we treat special cases when $\arg(\zeta) = -\frac{\pi}{4}, -\frac{\pi}{8}, -\frac{3\pi}{8}$, corresponding pure-gain-guiding [case (i)], the focusing thermal lens with gain guiding [case (ii)], and the defocusing lens with gain guiding [case (iii)]. The eigenvalues (ζ, β) for all three cases were calculated numerically, and the dependences of their real and imaginary parts (corresponding to the growth factor and frequency of every single mode) on the potential depth are shown in Fig. 2. We have calculated the first 10 modes (l, m) beyond the threshold. The first column in Fig. 2 represents a pure-gain-guiding case, where no lens is present. Each mode starts to exist when $\mathrm{Re}(i\beta^2) > 0$. Increasing the potential depth (or pump power) from zero to $|\zeta| \approx 1, 5$, the laser starts to generate the fundamental mode (0,0). Increasing the pump further, the growth rate $\mathrm{Re}(i\beta^2)$ increases, and the frequency decreases in the fundamental mode, while new modes (1, 0), (2, 0), (0, 1), (3, 0), (1, 1), (4, 0), (2, 1), (0, 2), and (5,0) start to emerge one after the other. More and more modes can potentially coexist together. Each new mode has a lower growth ratio $\mathrm{Re}(i\beta^2)$ and higher frequency $\mathrm{Im}(-i\beta^2)$ than the one before. Similar to the first column in Fig. 2, the second and third columns represent cases where the thermal lens is focusing and defocusing ($G_0 = \rho_0$, $G_0 = -\rho_0$, respectively). The tendencies are similar to those in the pure-gain-guiding case. The focusing lens reduces the generation threshold of the first mode, while the defocusing lens increases it ($|\zeta| \approx 1$ and $|\zeta| \approx 2$, respectively). The frequency of every single mode tends to increase and decrease for focusing and defocusing cases while increasing the pumping.

We depict the mode shape and the dependence of its beam quality factor M^2 on the potential-well depth $|\zeta|$ in Fig. 3. In the second row of Fig. 3 we represent the potential-well-depth

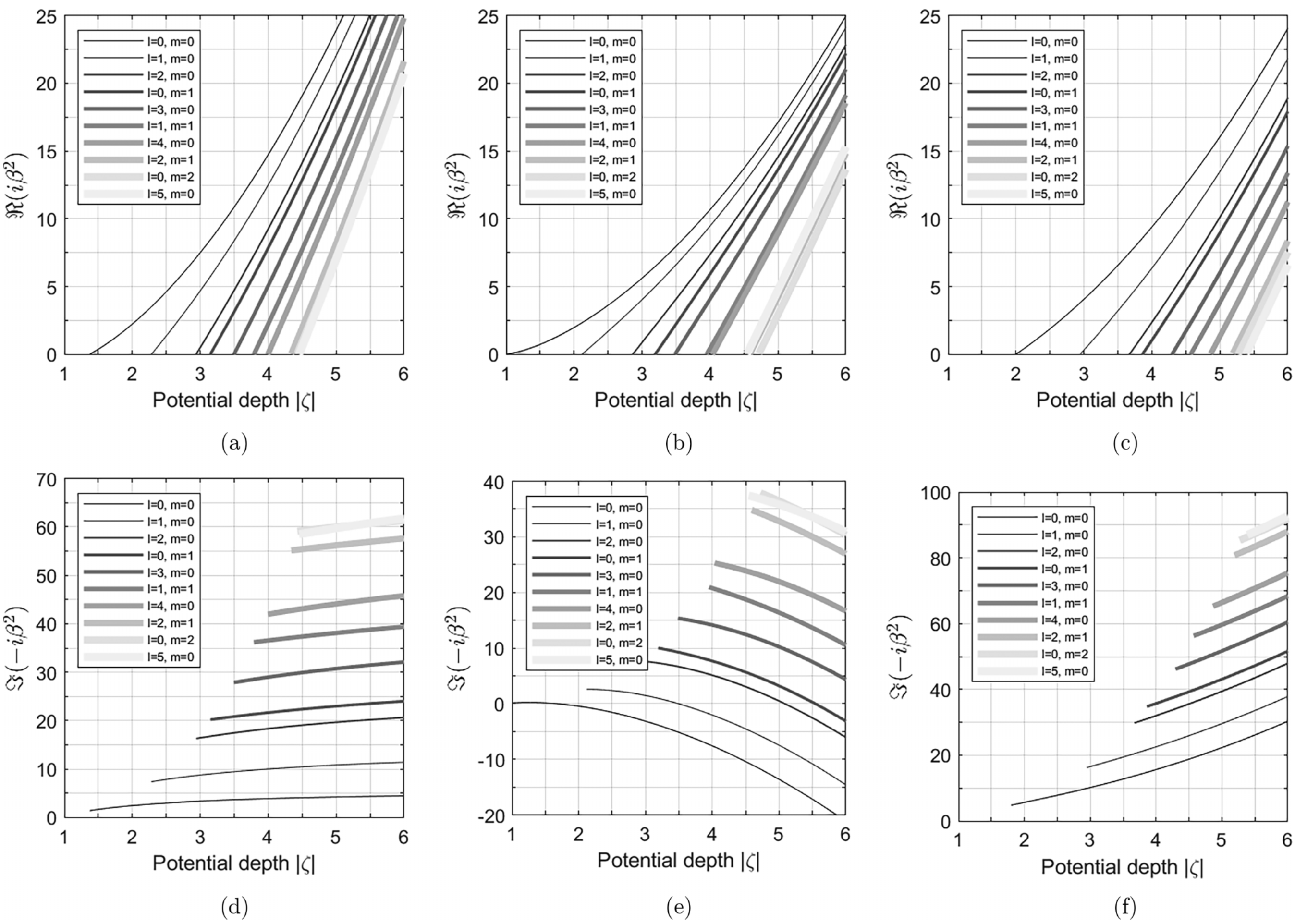

FIG. 2. The gain $\mathrm{Re}(i\beta^2)$ and frequency $\mathrm{Im}(-i\beta^2)$ dependences of the individual modes on the potential-well depth $|\zeta|$. In the columns three cases are shown: (a) and (d) without a thermal lens $\rho_0 = 0$, (b) and (e) with a focusing lens $\rho_0 = G_0$, and (c) and (f) with a defocusing lens $\rho_0 = -G_0$.

value $|\zeta|$ by a red dashed vertical line, and the ordinate axis scales only it. Meanwhile, the mode amplitudes are scaled to a fixed numerical value and are stacked vertically according to the sequence in which they come into existence, deepening the potential value of $|\zeta|$. Each value of $|\zeta|$ supports a unique set of transverse modes, which differ by amplitude and phase distribution. The abscissa axis scale is valid for both the potential well and mode amplitude, where the potential-well radius coincides with the pumping-cylinder radius. Here the corresponding eigenvalue pair (α, β) calculated from (11) represents the radial mode shape in (9). The radial part should be inserted into (2), so both the angular and radial parts can be represented. Once we know the electric-field distribution, we can apply the methodology provided in the Appendix and calculate the beam quality factor M^2.

In the first column of Fig. 3, we can see the beam quality factor M^2 and mode-shape dependence on the potential depth $|\zeta|$ because no lens is present, only gain. The mode shape in Fig. 3(d) is represented by the normalized electric-field absolute value $|A|$ and phase. The phase value is indicated by color in the radial part. We can see that the higher potential depth $|\zeta|$ means a higher quantity of modes localized in the well. If we increase the pump up to $|\zeta| \approx 1, 5$, the laser starts to generate the fundamental mode (0,0). The mode is spread widely, and its beam quality factor M^2 is high. With a further increase of the potential depth, the fundamental mode starts to localize better, and its beam quality factor M^2 reduces significantly, while its endings become steep. The higher modes (1, 0), (2, 0), (0, 1), (3, 0), (1, 1), (4, 0), (2, 1), (0, 2), and (5,0) follow the same pattern; they localize from infinity with high M^2, and their endings become steep as the pump increases.

Very similar to the first column in Fig 3, the second and third columns represent cases where the thermal lens is focusing and defocusing ($G_0 = \rho_0$, $G_0 = -\rho_0$, respectively). We see very similar tendencies as in the pure-gain-guiding case. In the case of the focusing lens, the mode endings are of weaker phase modulation than in the pure-gain-guiding case. Also, the modes are better localized at the same $|\zeta|$. The defocusing lens brings more phase modulation to the endings. The focusing lens reduces the generation threshold of the first mode.

IV. COMPOSITE BEAM QUALITY FACTOR M^2

In the previous section, we gave estimates of the dependence of the beam quality factor M^2 on the possible depth of $|\zeta|$ for each transverse mode (l, m). Here we calculate

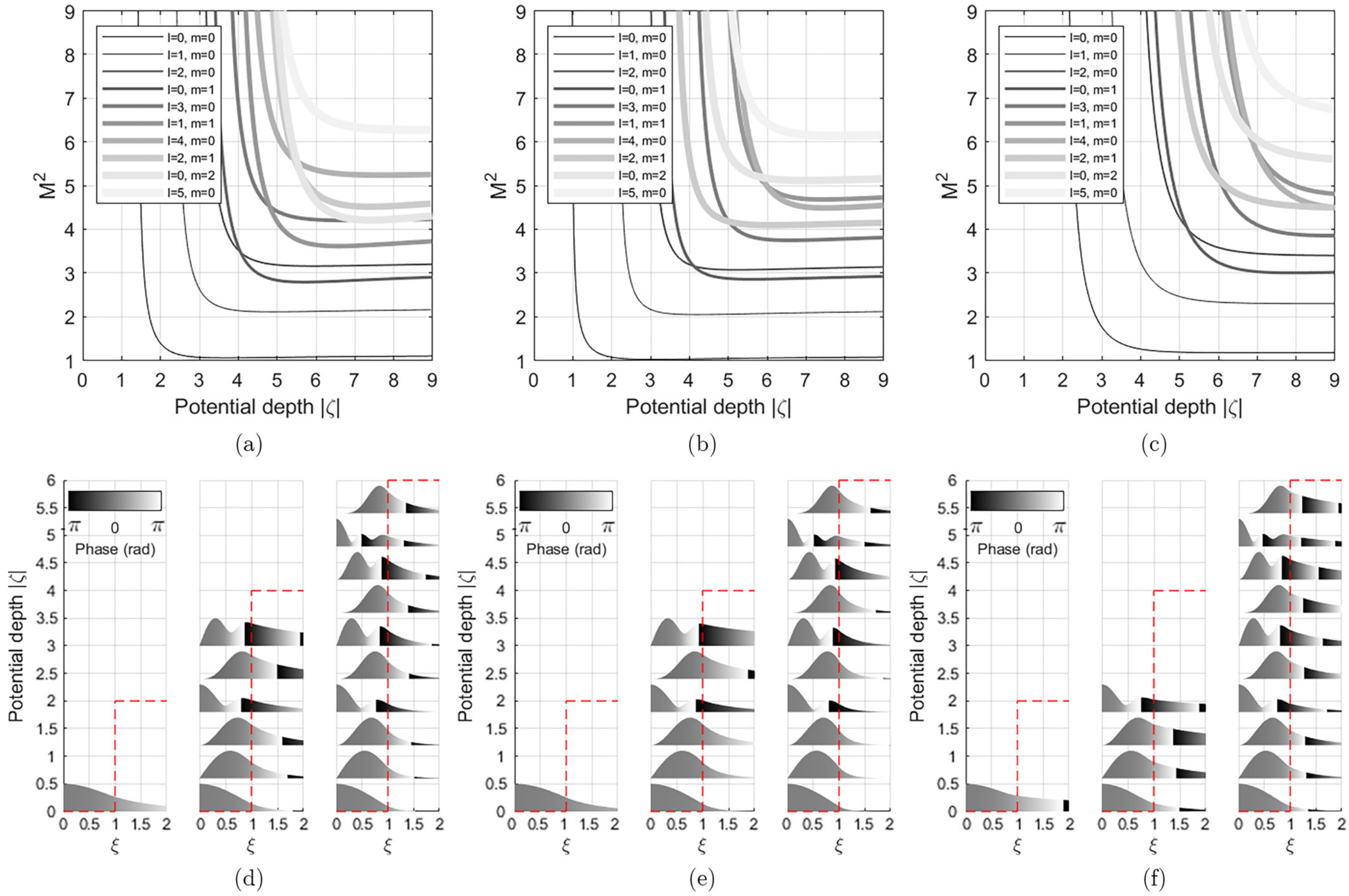

FIG. 3. The beam quality factors and beam shapes of each individual mode depending on potential-well depth $|\zeta|$. The mode shape is represented by the normalized electrical-field absolute value $|A|$ and phase, which is indicated by color in the range $(-\pi;\pi)$. The red dashed lines in (d)–(f) signify the potential well $|\zeta|$ in which the modes are localized, and the ordinate axis scales only it. Meanwhile, the mode amplitudes are scaled to a fixed numerical value and are stacked vertically according to the sequence in which they come into existence while deepening the potential $|\zeta|$. The abscissa axis scale is valid for both the potential well and mode amplitude, where the potential-well radius coincides with the pumping-cylinder radius. The plots in three columns represent the same cases as in Fig. 2.

the beam's composite beam quality factor M^2, consisting of multiple modes overlapping each other. We assume that our laser is of class B [25] and modes compete very weakly with each other. This assumption is only empirical and should also be verified with nonlinear analysis, which is beyond the scope of this paper. Following this assumption, we introduce an equation that could help with the preliminary estimate of the composite beam quality factor:

$$M^2 = \frac{\sum_{l,m}^{\infty} M_{lm}^2 (\lambda_{re})_{lm}}{\sum_{l,m}^{\infty} (\lambda_{re})_{lm}}, \tag{12}$$

where only the modes with positive $(\lambda_{re})_{lm}$ are considered. We have summed up the beam quality factor of every single mode M_{lm}^2 multiplied by its growth ratio $(\lambda_{re})_{lm}$ and normalized the result to the sum of the growth ratios. Equation (12) estimates the composite M^2 dependence on pumping for different resonator lengths and spots. Note that the eigenvalues of $(\zeta, \mathrm{Re}(i\beta^2))$ (already calculated in the previous section for three beam-guiding cases) along with relations (6) and (7) can be used to find growth rates $(\lambda_{re})_{lm}$ and beam quality factors M_{lm}^2 for every single mode.

In our experiment, we use a microchip laser with two different resonator round-trip lengths: $L_1 = 5$ mm and $L_2 = 15$ mm. Other parameters are as follows: pumping spot radius $R = 140\,\mu$m, laser wavelength of $1064\,\mu$m, Nd:yttrium aluminum garnet (YAG) crystal length of 2.3 mm (the same crystal is used in both cavities), refractive index $n = 1.81$, and losses per round trip $\rho = 0.0825$; the diffraction coefficient depends on the resonator round-trip length, so $d_1 = 4.67 \times 10^{-10}\,\mathrm{m}^2$, $d_2 = 2.16 \times 10^{-9}\,\mathrm{m}^2$. We estimate that in our experiments, the thermal-lens-induced phase modulation is negligible compared with gain per round trip ($\rho_0 \ll G_0$) and assume these are pure-gain-guiding cases. The λ_{re} and gain G_0 values calculated for this case are shown in the first column of Fig. 4 for both resonator lengths. The beam quality factor M^2 of every single mode is also recalculated analogically, and the results are shown in the middle column of Fig. 4. Here the dashed lines represent the states where no generation is present due to the negative growth factor $\lambda_{re} < 0$ of this particular transverse mode. The red squares represent the point where the mode starts to exist physically.

Now, considering the pumping power P is directly proportional to gain G_0, we normalize both parameters to their threshold values. This assumption allows us to relate our

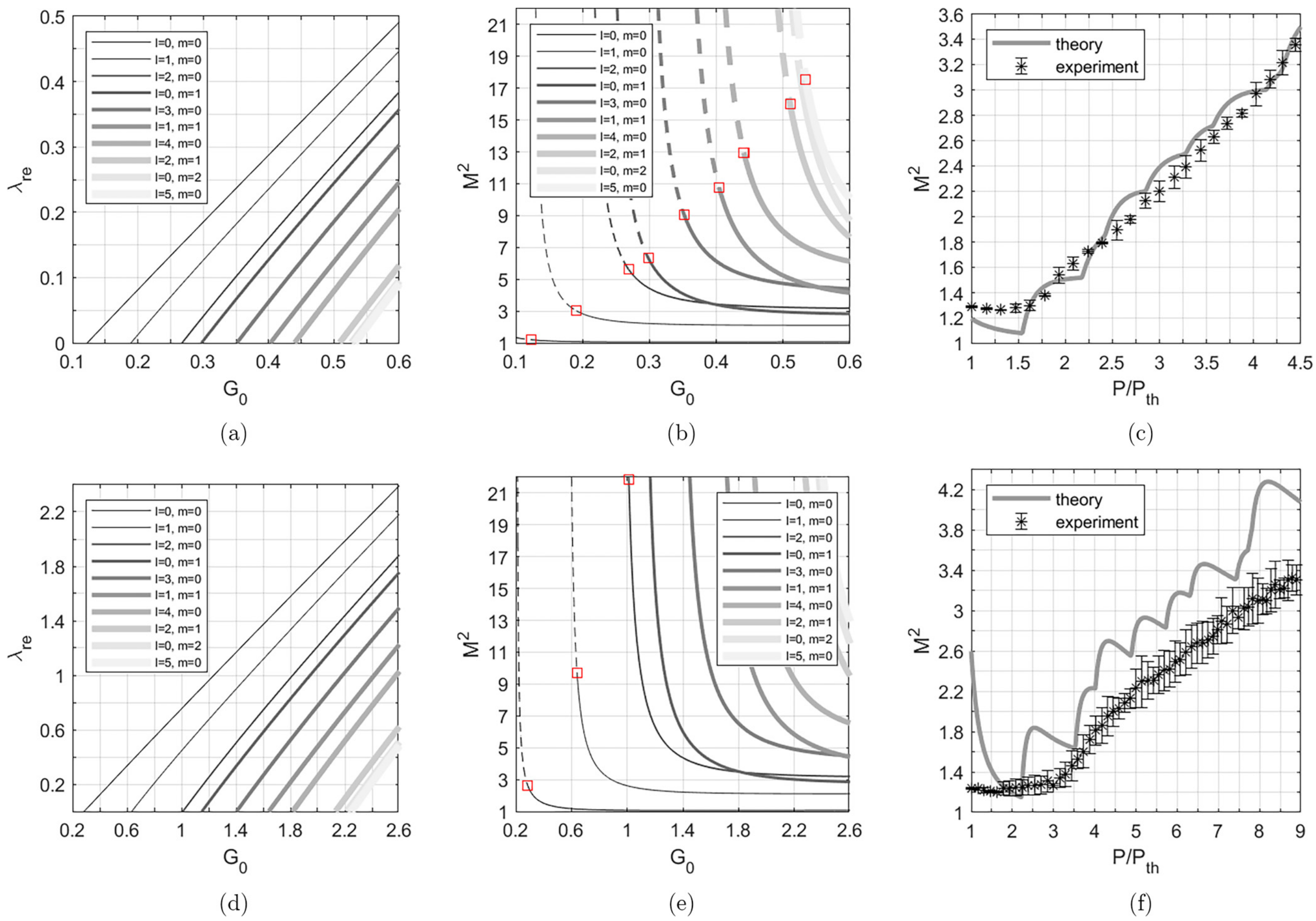

FIG. 4. (a) and (d) Growth ratio λ_{re}, (b) and (e) single-mode beam quality factor, and (c) and (f) composite beam quality factor dependences on gain G_0 and pump power P/P_{th} over the generation threshold P_{th}. The first and second rows correspond to different resonator round-trip lengths, $L = 5$ mm and $L = 15$ mm, respectively. The gray curves in (c) and (f) represent the theoretically estimated M^2, while the black stars with error bars show experimentally measured values. The dashed lines in (b) and (e) represent the states where no generation is present due to the negative growth factor $\lambda_{re} < 0$ of this particular transverse mode. The red squares represent the point where the mode starts physically to exist.

experiment to theory. Calculated from (12), the dependence of the composite beam quality factor M^2 on pump power is provided in the third column of Fig. 4 as the gray curve for both resonator lengths. Measured according to International Organization for Standardization Standard 11146 [26], the beam quality factor M^2 is depicted here as black stars with error bars. The shorter-cavity experimental data find better agreement with the theoretical curve than the data for the longer one. One can recognize the slight vertical shift and undulations. In our understanding, the longer resonator generates modes of weaker localization and higher beam quality factors at the threshold. Weakly localized modes contain higher M^2 factors and make a rapid contribution to the composite beam quality factor, increasing the pump power. Accordingly, the major undulations are observed in the longer cavity's theoretical and experimental curves. On the other hand, less localized modes are more sensitive to crystal aperture, which is not included in the theoretical model. That could contribute to the vertical offset. It is worth mentioning that the mean-field approximation fits the shorter cavities better. Due to the large contribution of free space in the longer cavity (4.6-mm Nd:YAG crystal and 10.4-mm free space), the gain is distributed very unevenly along the cavity axis, and this is not included in our theoretical model. Despite the discrepancies noted, the theoretical and experimental results overlap adequately and allow us to claim that the method is suitable for a rough estimation of laser beam quality factor M^2 at various pump powers in a microchip laser.

V. CONCLUSIONS

In conclusion, we have investigated the influence of several physical effects and parameters on the beam quality of the flat-flat mirror microchip laser analytically. For this reason, the two-dimensional linear field equation was introduced using cylindric symmetry and a mean-field approximation. The physical effects accounting for this analysis of laser beam formation were the gain, thermal lens, diffraction, and losses. In this case, the equation becomes similar to the Schrödinger wave equation with a finite potential barrier, which is complex in our case. We found the eigenvalues and eigenfunctions (corresponding to mode shapes) for three specific cases and evaluated beam quality factors M^2 and growth ratios λ_{re} for each separate mode. For simplicity, we introduced an equation that allows a rough estimation of the composite (multiple modes) beam quality factor M^2, disregarding the competition of generated modes. Calculated M^2 values were compared to experimental ones, and satisfactory agreement was found.

ACKNOWLEDGMENTS

This work has received funding from the Spanish Ministerio de Ciencia e Innovación under Grants No. PID2019 and 109175GB-C21, and the European Social Fund (Project No. 09.3.3- LMT-K712-17- 0016) under a grant agreement with the Research Council of Lithuania (LMTLT). Authors are grateful to Tadas Lipinskas (OPTOGAMA UAB) for valuable advice and support.

APPENDIX: BEAM QUALITY M^2 OF THE SINGLE-MODE CALCULATION IN A MICROCHIP LASER

Here we estimate the single-mode beam quality M^2 from the phase and amplitude distribution in the transverse plane of a particular mode electric field $A(r, \phi)$. The task would be easy if the electric field were in the waist plane and we could calculate it using $M^2 = 4\pi\sigma_0\sigma_s$ [27], where σ_0^2 and σ_s^2 are the field second moments in the space and Fourier domains, respectively. However, in our case, the field distribution is complex (α and β coefficients are complex), and the field distribution given is outside the waist. The analytical way to calculate the beam quality in two dimensions outside the waist was suggested by Yoda *et al.* [28]. Briefly, instructions are as follows: one should calculate the first and second moments,

$$\langle x\rangle = \iint x dx dy |A(x, y)|^2, \tag{A1}$$

$$\sigma_x^2 = \iint dx dy (x - \langle x\rangle)^2 |A(x, y)|^2. \tag{A2}$$

Additionally, one should calculate the auxiliary integrals A and B:

$$A = \iint dx dy (x - \langle x\rangle)\left[A(x, y)\frac{\partial A(x, y)*}{\partial x} - \text{c.c.}\right], \tag{A3}$$

$$B = \iint dx dy \left|\frac{\partial A(x, y)}{\partial x}\right|^2 + \frac{1}{4} \times \left(\iint dx dy \left[A(x, y)\frac{\partial A(x, y)*}{\partial x} - \text{c.c.}\right]\right)^2. \tag{A4}$$

One should note that the complex-conjugate member should be calculated only in the square brackets. Finally, one should use the A, B, and σ_x^2 values in the final M_x^2 expression:

$$M_x^2 = \sqrt{4B\sigma_x^2 + A^2}. \tag{A5}$$

Equation (A5) is valid for beams out of the waist plane. If it is applied to the waist plane where the electric field is real, the calculations will simplify because the last term in the B expression (A4) vanishes.

[1] H. Kogelnik and T. Li, Laser beams and resonators, Appl. Opt. **5**, 1550 (1966).

[2] A. E. Siegman, *Lasers* (University Science Books, Sausalito, California, 1986).

[3] H. Haken, *Laser Light Dynamics* (North-Holland Physics Publishing, Amsterdam, Holland, 1985), Vol. 2.

[4] K. Staliunas and V. J. Sanchez-Morcillo, *Transverse Patterns in Nonlinear Optical Resonators* (Springer, Heidelberg, 2002).

[5] L. A. Lugiato, F. Prati, and M. Brambilla, *Nonlinear Optical Systems* (Cambridge University Press, Cambridge, 2015).

[6] A. Bassi, F. Prati, and L. A. Lugiato, Optical instabilities in Fabry-Perot resonators, Phys. Rev. A **103**, 053519 (2021).

[7] F. Prati, L. A. Lugiato, A. Gatti, L. Columbo, C. Silvestri, M. Gioannini, M. Brambilla, M. Piccardo, and F. Capasso, Global and localised temporal structures in driven ring quantum cascade lasers, Chaos, Solitons Fractals **153**, 111537 (2021).

[8] A. E. Siegman, Hermite–Gaussian functions of complex argument as optical-beam eigenfunctions, J. Opt. Soc. Am. **63**, 1093 (1973).

[9] J. J. Zayhowski and A. Mooradian, Single-frequency microchip Nd lasers, Opt. Lett. **14**, 24 (1989).

[10] G. K. Harkness and W. J. Firth, Transverse modes of microchip solid state lasers, J. Mod. Opt. **39**, 2023 (1992).

[11] S. Longhi, Theory of transverse modes in end-pumped microchip lasers, J. Opt. Soc. Am. B **11**, 1098 (1994).

[12] S. Longhi and P. Laporta, Longitudinal–transverse mode interplay and conical emission in microchip lasers, J. Opt. Soc. Am. B **12**, 1511 (1995).

[13] F. Sanchez and A. Chardon, Transverse modes in microchip lasers, J. Opt. Soc. Am. B **13**, 2869 (1996).

[14] F. Sanchez and A. Chardon, Pump size optimization in microchip lasers, Opt. Commun. **136**, 405 (1997).

[15] C. Serrat, M. P. van Exter, N. J. van Druten, and J. P. Woerdman, Transverse mode formation in microlasers by combined gain- and index-guiding, IEEE J. Quantum Electron. **35**, 1314 (1999).

[16] N. J. van Druten, Observation of transverse modes in a microchip laser with combined gain and index guiding, J. Opt. Soc. Am. B **13**, 2869 (2001).

[17] L. Cini and J. I. Mackenzie, Analytical thermal model for end-pumped solid-state lasers, Appl. Phys. B **123**, 273 (2017).

[18] M. Achtenhagen, A. A. Hardy, and E. Kapon, Threshold analysis of vertical-cavity surface-emitting lasers with intracavity contacts, IEEE J. Quantum Electron. **42**, 889 (2006).

[19] O. Conradi, S. Helfert, and R. Pregla, Comprehensive modeling of vertical-cavity laser-diodes by the method of lines, IEEE J. Quantum Electron. **37**, 928 (2001).

[20] G. R. Hadley, M. E. Warren, K. D. Choquette, J. W. Scott, and S. W. Corzine, Comprehensive numerical modeling of vertical-cavity surface-emitting lasers, IEEE J. Quantum Electron. **32**, 607 (1996).

[21] S. Longhi, Airy beams from a microchip laser, Opt. Lett. **36**, 716 (2011).

[22] S. Liu, F. Song, H. Cai, T. Li, B. Tian, Z. Wu, and J. Tian, Effect of thermal lens on beam quality and mode matching in LD pumped Er–Yb-codoped phosphate glass microchip laser, J. Phys. D **41**, 035104 (2008).

[23] M. Tsunekane and T. Taira, 300 W continuous-wave operation of a diode edge-pumped, hybrid composite Yb:YAG microchip laser, Opt. Lett. **31**, 2003 (2006).

[24] M. Abramowitz and I. A. Stegun, *Handbook of Mathematical Functions with Formulas, Graphs, and Mathematical Tables* (National Bureau of Standards, Washington, DC, 1972).

[25] K. Staliunas, M. F. H. Tarroja, and C. O. Weiss, Transverse mode locking, antilocking and self-induced dynamics of class-B lasers, Opt. Commun. **102**, 69 (1993).

[26] International Standards Organization (ISO), Lasers and Laser-Related Equipment: Test methods for laser beam widths, divergence angles and beam propagation ratios, ISO 11146-1:2005 (International Standards Organization, Geneva, 2005).

[27] A. E. Siegman, Defining the effective radius of curvature for a nonideal optical beam, IEEE J. Quantum Electron. **27**, 1146 (1991).

[28] H. Yoda, P. Polynkin, and M. Mansuripur, Beam quality factor of higher order modes in a step-index fiber, J. Lightwave Technol. **24**, 1350 (2006).